AMERICAN SOCIETY FOR MICROBIOLOGY | Applied and Environmental Microbiology

Applied and Industrial Microbiology | Full-Length Text

Optimization of $IspS_{ib}$ stability through directed evolution to improve isoprene production

Meijie Li,[1] Rumeng Yang,[1] Jing Guo,[2,3,4] Min Liu,[5] Jianming Yang[1]

AUTHOR AFFILIATIONS See affiliation list on p. 16.

ABSTRACT Enzyme stability is often a limiting factor in the microbial production of high-value-added chemicals and commercial enzymes. A previous study by our research group revealed that the unstable isoprene synthase from *Ipomoea batatas* ($IspS_{ib}$) critically limits isoprene production in engineered *Escherichia coli*. Directed evolution was, therefore, performed in the present study to improve the thermostability of $IspS_{ib}$. First, a tripartite protein folding system designated as lac′-$IspS_{ib}$-′lac, which could couple the stability of $IspS_{ib}$ to antibiotic ampicillin resistance, was successfully constructed for the high-throughput screening of variants. Directed evolution of $IspS_{ib}$ was then performed through two rounds of random mutation and site-saturation mutation, which produced three variants with higher stability: $IspS_{ib}^{N397V\ A476V}$, $IspS_{ib}^{N397V\ A476T}$, and $IspS_{ib}^{N397V\ A476C}$. The subsequent *in vitro* thermostability test confirmed the increased protein stability. The melting temperatures of the screened variants $IspS_{ib}^{N397V\ A476V}$, $IspS_{ib}^{N397V\ A476T}$, and $IspS_{ib}^{N397V\ A476C}$ were 45.1 ± 0.9°C, 46.1 ± 0.7°C, and 47.2 ± 0.3°C, respectively, each of which was higher than the melting temperature of wild-type $IspS_{ib}$ (41.5 ± 0.4°C). The production of isoprene at the shake-flask fermentation level was increased by 1.94-folds, to 1,335 mg/L, when using $IspS_{ib}^{N397V\ A476T}$. These findings provide insights into the optimization of the thermostability of terpene synthases, which are key enzymes for isoprenoid production in engineered microorganisms. In addition, the present study would serve as a successful example of improving enzyme stability without requiring detailed structural information or catalytic reaction mechanisms.

IMPORTANCE The poor thermostability of $IspS_{ib}$ critically limits isoprene production in engineered *Escherichia coli*. A tripartite protein folding system designated as lac'-$IspS_{ib}$-'lac, which could couple the stability of $IspS_{ib}$ to antibiotic ampicillin resistance, was successfully constructed for the first time. In order to improve the enzyme stability of $IspS_{ib}$, the directed evolution of $IspS_{ib}$ was performed through error-PCR, and high-throughput screening was realized using the lac'-$IspS_{ib}$-'lac system. Three positive variants with increased thermostability were obtained. The thermostability test and the melting temperature analysis confirmed the increased stability of the enzyme. The production of isoprene was increased by 1.94-folds, to 1,335 mg/L, using $IspS_{ib}^{N397V\ A476T}$. The directed evolution process reported here is also applicable to other terpene synthases key to isoprenoid production.

KEYWORDS isoprene synthase, enzyme stability, directed evolution, isoprene production, isoprenoid, biosensor

Isoprene is a chemical used widely in the production of synthetic rubber (95%), as well as various other compounds (the remaining 5%), including pesticides, pharmaceuticals, oil additives, adhesives, fragrances, and biofuels (1, 2). Most of the commercial isoprene is currently produced through the chemical cracking of petroleum, a process that is environmentally unfriendly, price-unstable, unsustainable, and energy-intensive

Editor Marina Lotti, University of Milano-Bicocca, Milano, Italy

Address correspondence to Jianming Yang, yjming888@126.com.

Meijie Li and Rumeng Yang contributed equally to this article. Meijie Li was the major contributor to the preparation of the text and so is listed first.

The authors declare no conflict of interest.

See the funding table on p. 16.

Received 15 July 2023
Accepted 11 August 2023
Published 10 October 2023

(3). Microbial production of isoprene is an alternative, and considerable effort has been invested in improving the production of isoprene using this method (4–6). Isoprene can be synthesized from dimethylallyl diphosphate (DMAPP) under the catalysis of isoprene synthase (IspS) present in plants and certain microbes (7). The precursor DAMPP is synthesized via the methylerythritol phosphate (MEP) pathway or the mevalonate (MVA) pathway (8). In the process of isoprene production in *Escherichia coli*, heterologous overexpression of IspS is necessary, for which the overexpression of genes involved in the MVA pathway is usually used as a strategy to improve the metabolic flux for the accumulation of the precursor DMAPP (9). The metabolic flux is further improved, usually through the reduction of the byproducts for the accumulation of the precursor acetyl-CoA, manipulation of gene expression through promoters and optimization of RBSs, directed evolution of key enzymes, and exploration of the novel MVA pathway (10). A study reported that the *E. coli* strain AceCo, which exhibited the formation of reduced byproducts and had the IspS gene and the MVA pathway, exhibited the highest production of isoprene (1,832 mg/L) in shake-flask culture (2). Another *E. coli* strain, which double expressed the MVA pathway genes, exhibited isoprene production of approximately 25.2 g/L under scale-up fed-batch fermentation (300 L) (11).

IspS is reported as the rate-limiting enzyme in the isoprene synthetic pathway (7). Most of the reported IspS enzymes exhibit low activity, substrate affinity, and thermal stability (4, 12). In a previous study by our research group (4), the IspS from *Ipomoea batatas* ($IspS_{ib}$) was utilized for isoprene production. In another study, $IspS_{ib}$ exhibited a relatively higher catalytic efficiency than the IspSs from other species and also led to high isoprene production (7). However, $IspS_{ib}$ was also revealed as a thermally unstable enzyme *in vitro* as well as *in vivo* (7). The correlation between $IspS_{ib}$ expression and isoprene productivity during the fermentation process indicated that the instability of $IspS_{ib}$ critically affected the production of isoprene (4, 7). The enzyme activity of purified $IspS_{ib}$ declined rapidly, reaching 20% of the initial enzyme activity after just 20 min of incubation at 30°C, indicating the thermal instability of $IspS_{ib}$ (7). Therefore, to further improve the production of isoprene, optimization of $IspS_{ib}$ stability is necessary.

Directed evolution and rational design are usually used for enzyme engineering aimed at improving catalytic activity, substrate selectivity, and enzyme stability (13). However, rational design requires detailed information on the structure and the catalytic reaction mechanism of the enzyme (14). The crystal structure of $IspS_{ib}$ has not been resolved to date, and among all kinds of IspSs from different species, only the structure of the IspS from gray poplar has been reported (15). The three-dimensional structure of $IspS_{ib}$ may be deciphered based on the structure of the IspS from gray poplar using homology modeling. Therefore, rational design is a selectable strategy for the engineering of $IspS_{ib}$. Directed evolution, on the other hand, does not depend on information on the structure and reaction mechanism of the enzyme. However, this approach requires the construction of an efficient, high-throughput screening method. Directed evolution of the IspS from *Populus alba* for enhancing the catalytic activity of this enzyme has been reported in a previous study, in which a high-throughput method based on DMAPP toxicity relief for achieving enhanced IspS catalytic activity was established (16). Therefore, directed evolution is a feasible strategy to improve the stability of $IspS_{ib}$ if an efficient high-throughput screening method is established.

Directed evolution is an efficient approach to improving protein stability (or folding) *in vivo* (17). This method involves the generation of a pool of variants, followed by a screening process to identify which of the generated variants exhibit improved folding properties. The accuracy, power, throughput, and stringency of the selection and screening methods are crucial to the success of the evolution process. A few selection and screening systems developed for improved protein folding include the inherent function of the protein, fusion to a reporter tag, tripartite protein folding sensors, and the twin arginine translocation system (17). A tripartite protein folding sensor method involves inserting the protein of interest between the split halves of an antibiotic resistance gene, and this method directly links the stability of the protein to its

antibiotic resistance (18). The two parts of the antibiotic resistance protein would only be able to fold together if the inserted protein folded suitably, resulting in resistance to antibiotics. If the inserted protein is poorly folded, it would be degraded by the proteases present inside the cell, and the two halves of the antibiotic resistance protein would separate, resulting in sensitivity to antibiotics. Therefore, this tripartite protein folding sensor enables efficient "fold or die" selection, which ensures improved stability.

In the present study, the directed evolution of $IspS_{ib}$ was performed to improve the stability of this enzyme. A tripartite protein folding sensor, which correlates the stability of $IspS_{ib}$ to its antibiotic resistance, was first developed and then used as the high-throughput screening method for the directed evolution of $IspS_{ib}$ to improve its stability. The stability of the obtained $IspS_{ib}$ variants was then evaluated through the thermostability test and the circular dichroism (CD) analysis. Finally, the effect of the selected $IspS_{ib}$ variants on isoprene production in engineered *E. coli* was investigated.

MATERIALS AND METHODS

Construction of the biosensor

E. coli DH5α was used for genetic manipulation. All primers used for the construction of plasmids are listed in Table 1. All plasmids used in this study are listed in Table 2. The ptrc-low (9) harboring the β-lactamase (lac) sequence was used as a template to amplify the N-terminal lac using the N-lac-F/R primers and the C-terminal lac using the C-lac-F/R primers. $IspS_{ib}$ was amplified using the $IspS_{ib}$-lac-F/R primers and the plasmid pA-MM-$IspS_{ib}$ as the template (4). Two rounds of overlap PCR were performed to insert $IspS_{ib}$ into lac, generating the fragment lac′-$IspS_{ib}$-′lac, which was then seamlessly cloned into the *Bgl* II and *Sac* I sites in the pET-28a plasmid, resulting in pET-$IspS_{ib}$-lac. Next, pET-$IspS_{ib}$-lac was transformed into *E. coli* BL21 (DE3) to obtain the biosensor for achieving $IspS_{ib}$ stability. A plasmid named pET-$IspS_{ib}$-linker-lac, which expressed the $IspS_{ib}$-lac fusion

TABLE 1 Primers used for plasmid construction

Primers	Sequences
N-lac-F	TAGAGGATCGAGATCTCGATTGCGTTTCTACAAACTCTTTTTGT
N-lac-R	AACCACCACCACCAGAACCACCACCACCtagttcgccagttaatagtttgcg
C-lac-F	GGGAGCGGAGGCGGCGGATCAGGCGGAGGTGGAAGCTTGactctagcttcccggcaaca
C-lac-R	CAAGCTTGTCGACGGAGCTCttaccaatgcttaatcagtgaggcac
$IspS_{ib}$-lac-F	TGGTTCTGGTGGTGGTGGTTCTTCCTCAGGTTCCGGGatgagtagcgcccagaatcag
$IspS_{ib}$-lac-R	GATCCGCCGCCTCCGCTCCCACTTCCGCTttcaaccggattaataataacgctaac
N-$IspS_{ib}$-F	CAAGCTTGTCGACGGAGCTCTTAttcaaccggattaataataacgctaac
N-$IspS_{ib}$-R	tggGGAGGAGGAGGAAGTatgagtagcgcccagaatcag
N-whole-lac-F	catACTTCCTCCTCCTCCcaatgcttaatcagtgaggc
N-whole-lac-R	TGCTTCAATAATATTGAAAAAGGAAGAGTatgagtattcaacatttccgtgtc
C-whole-lac-F	CAAGCTTGTCGACGGAGCTCttaccaatgcttaatcagtgaggcac
C-whole-lac-R	gaaGGAGGAGGAGGAAGTatgagtattcaacatttccgtgtcg
C-$IspS_{ib}$-F	catACTTCCTCCTCCTCCttcaaccggattaataataacgctaac
C-$IspS_{ib}$-R	TGCTTCAATAATATTGAAAAAGGAAGAGTatgagtagcgcccagaatcag
pET-F	ACTCTTCCTTTTTCAATATTATTGAAGCA
pET-R	GAGCTCCGTCGACAAGCTTG
$IspS_{ib}$-mtlibrary-F	CCCACTTCCGCTttcaaccg
$IspS_{ib}$-mtlibrary-R	atgagtagcgcccagaatcag
P-mtlibrary-F	ctgattctgggcgctactcat
P-mtlibrary-R	cggttgaaAGCGGAAGTGGG
$IspS_{ib}$-cx-F	ggaagctagagtCAAGCTTCCAC
$IspS_{ib}$-cx-R	gcgcaaactattaactggcg
$IspS_{ib}$-F	tataagaaggagatatacatatgagtagcgcccagaatcag
$IspS_{ib}$-R	ccgatatccaattgagatctttattcaaccggattaataataacgctaacaatac

TABLE 2 Strains and plasmids constructed in this work

Names	Description	References
Plasmids		
pACYCDuet-1	lacI; expression vector; T7 promoter; Cm^r	This study
pA-MM-$IspS_{ib}$	pACYCduet-1 carrying *mvaE* and *mvaS* from *Enterococcus faecalis*, $IspS_{ib}$ from *Ipomoea batatas*; Cm^r	(4)
ptrc-low	pYJM14, pTrcHis2B carrying ERG12, ERG8, ERG19, and IDI from *S. cerevisiae*; Amp^r	(6)
pACYC-$IspS_{ib}$	pACYCduet-1 carrying $IspS_{ib}$ from *Ipomoea batatas*; Cm^r	(7)
pET-$IspS_{ib}$-lac	IspSib was inserted between the N-terminal and C-terminal of the reporter gene β-lac; Amp^r	This study
pET-$IspS_{ib}$-linker-lac	Fusion enzyme $IspS_{ib}$-lac; Amp^r and Km^r	This study
pET-lac-linker-$IspS_{ib}$	Fusion enzyme lac-$IspS_{ib}$; Amp^r and Km^r	This study
pACYC-$IspS_{ib}^{N397V\ A476V}$	pACYCDuet-1 carrying $IspS_{ib}^{N397V\ A476V}$	This study
pACYC-$IspS_{ib}^{N397V\ A476T}$	pACYCDuet-1 carrying $IspS_{ib}^{N397V\ A476T}$	This study
pACYC-$IspS_{ib}^{N397V\ A476C}$	pACYCDuet-1 carrying $IspS_{ib}^{N397V\ A476C}$	This study
pA-MM-$IspS_{ib}^{N397V\ A476V}$	Derived from pACYC-mvaE-mvaS-$IspS_{ib}$, with variant $IspS_{ib}^{N397V\ A476V}$	This study
pA-MM-$IspS_{ib}^{N397V\ A476T}$	Derived from pACYC-mvaE-mvaS-$IspS_{ib}$, with variant $IspS_{ib}^{N397V\ A476T}$	This study
pA-MM-$IspS_{ib}^{N397V\ A476C}$	Derived from pACYC-mvaE-mvaS-$IspS_{ib}$, with variant $IspS_{ib}^{N397V\ A476C}$	This study
Strains		
E. coli BL21 (DE3)	F– *ompT hsdSB*(rB– mB–) *gal dcm*(DE3)	Invitrogen
$IspS_{ib}$ stability biosensor	*E. coli* Bl21(DE3)/pET-$IspS_{ib}$-lac	This study
EISO01	*E. coli* Bl21(DE3)/pACYC-$IspS_{ib}$	This study
EISO02	*E. coli* Bl21(DE3)/pACYC-$IspS_{ib}^{N397V\ A476V}$	This study
EISO03	*E. coli* Bl21(DE3)/pACYC -$IspS_{ib}^{N397V\ A476T}$	This study
EISO04	*E. coli* Bl21(DE3)/pACYC -$IspS_{ib}^{N397V\ A476C}$	This study
EISO05	*E. coli* Bl21(DE3)/ptrc-low / pA-MM-$IspS_{ib}$	This study
EISO06	*E. coli* Bl21(DE3)/ptrc-low / pA-MM-$IspS_{ib}^{N397V\ A476V}$	This study
EISO07	*E. coli* Bl21(DE3)/ptrc-low / pA-MM-$IspS_{ib}^{N397V\ A476T}$	This study
EISO08	*E. coli* Bl21(DE3)/ptrc-low / pA-MM-$IspS_{ib}^{N397V\ A476C}$	This study

enzyme with $IspS_{ib}$ at the N-terminal of the whole lac, was constructed for use as the control. The plasmid pET-lac-linker-$IspS_{ib}$ expressing the lac-$IspS_{ib}$ fusion enzyme, in which $IspS_{ib}$ was located at the C-terminal of the whole lac, was also constructed. The construction processes are detailed in the supplementary file.

In order to determine the level of antibiotic resistance of the constructed biosensor, a few tests were conducted. The biosensor was inoculated into the lysogeny broth (LB) medium containing 50 mg/L of kanamycin and increasing concentrations of the antibiotic ampicillin, including 0, 20, 40, 60, 80, and 100 mg/L. Afterward, OD_{600} was measured every 2 h. Spot titer tests were performed by spotting the serial dilutions of the mid-log-phase biosensor cells onto the LB plates supplemented with 50 mg/L of kanamycin and increasing concentrations of ampicillin, including 0, 20, 40, 60, 80, and 100 mg/L. The serial dilutions of the mid-log-phase biosensor cells were also spread onto the LB plates supplemented with 50 mg/L of kanamycin and increasing concentrations of ampicillin, including 10, 20, 30, 40, and 50 mg/L.

Directed evolution

Error-prone PCR was performed to obtain the mutant $IspS_{ib}$. The $IspS_{ib}$-mtlibrary-F/R primers were used for the amplification of $IspS_{ib}$ using the 2× Taq Plus Master Mix II (Vazyme Biotech), 100 mM $MgCl_2$, and 10 mM $MnCl_2$. The carrier pET-$IspS_{ib}$-lac was amplified using the P-mtlibrary-F and P-mtlibrary-R primers. Afterward, the two PCR fragments were seamlessly assembled, and the mixture was transformed into *E. coli* DH5α to obtain the mutant library. The mutant library was then spread onto the LB plates supplemented with 40 mg/L of ampicillin for the variant selection process, and

50 mg/L of kanamycin was also added to detect the presence of the plasmid. The single clones were streaked using a sterile toothpick onto plated LB medium containing 40 mg/L of ampicillin and 50 mg/L of kanamycin for the confirmation of cell growth. Colony PCR was performed for the obtained single clones using the $IspS_{ib}$-cx-F/R primers, and the single clones that exhibited the whole $IspS_{ib}$ fragments were selected for further analysis. The obtained positive clones were then inoculated in a fluid LB medium containing 50 mg/L of kanamycin and different concentrations of ampicillin, including 20, 40, and 60 mg/L, followed by an OD_{600} measurement. The single clones exhibiting high cell growth were selected.

Site-directed mutagenesis

The positive single clones obtained through random mutation screening were sequenced, which revealed several mutation sites (such as $IspS_{ib}^{V406A\ N397S\ T388A}$). In order to confirm the key mutation sites, the variants with a single mutation site, such as $IspS_{ib}^{V406A}$, $IspS_{ib}^{N397S}$, and $IspS_{ib}^{T388A}$, were constructed based on pET-$IspS_{ib}$-lac using the Fast Site-Directed Mutagenesis Kit (Tigen, China). After confirmation, the key mutation sites, such as N397 and A476, were mutated to other 19 amino acids using the Fast Site-Directed Mutagenesis Kit (Tigen, China), thereby generating a site-saturated mutant library. The obtained clones were evaluated for cell growth in the LB medium containing 40 mg/L of ampicillin and 50 mg/L of kanamycin.

Enzyme thermostability test

In order to achieve enzyme expression, plasmids have to be constructed first. Using pACYC-$IspS_{ib}^{N397V\ A476V}$ as an example, the wild-type $IspS_{ib}$ in the pACYC-$IspS_{ib}$ plasmid (7) was mutated to $IspS_{ib}^{N397V\ A476V}$ through two rounds of site-directed mutagenesis, thereby generating pACYC-$IspS_{ib}^{N397V\ A476V}$, which was then transformed into *E. coli* BL21 (DE3). The culture process for enzyme expression, the enzyme purification process, and the SDS-PAGE process are described in another report (7). Protein concentration was quantified using the Bradford assay (Beyotime, China). The purified enzyme was incubated at 30°C, 40°C, and 50°C, respectively, and then sampled for 10, 20, 40, and 60 min to determine the IspS enzyme activity. The process for determining IspS activity is detailed in a previously published report (7).

CD analysis

The thermal melting temperature (T_m) of the proteins was determined using a circular dichroism spectrometer (Chirascan, Applied Photophysics Ltd., English) and a 0.5-mm quartz colorimeter. In these measurements, the wavelength range used was 195 to 260 nm, the bandwidth and the step length were set to 1 nm, and the scanning speed was 2 s/nm (19). In order to determine the appropriate protein concentration, the purified protein was first diluted in PBS to concentrations of 0.025, 0.050, 0.100, 0.25, and 0.500 mg/mL, following which the CD absorption spectra of the four protein solutions were obtained in the wavelength range of 195–260 nm and a temperature range of 20°C–60°C, once per degree. The CD value (millidegrees, mdeg) was converted to mean residue ellipticity ([θ]), which represented the read-two optical absorption value (20) [θ] and was calculated as follows:

$$[\theta] = \theta \cdot M/(l \cdot c \cdot n_r)$$

In the above equation, θ denotes the observed ellipticity, M is the molecular mass of $IspS_{ib}$, l denotes the pathlength (mm), c is the concentration of $IspS_{ib}$ (mg/mL), and n_r is the number of amino acids. The T_m value was determined through the Global3 analysis of the CD spectrum.

Fermentation

The first step of isoprene production was replacing the wild-type $IspS_{ib}$ in plasmid pA-MM-$IspS_{ib}$ (4) with $IspS_{ib}$ variants, namely, $IspS_{ib}^{N397V\ A476V}$, $IspS_{ib}^{N397V\ A476T}$, and $IspS_{ib}^{N397V\ A476C}$. Using the construction of pA-MM-$IspS_{ib}^{N397V\ A476V}$ as an example, the fragment $IspS_{ib}^{N397V\ A476V}$ was PCR-amplified using primers $IspS_{ib}^{N397V\ A476V}$-F/R and then seamlessly cloned into the *Bgl* II and *Nde* I sites of pA-MM-$IspS_{ib}$, which was linearized using a restriction enzyme. Strain EISO06 was constructed through the co-transformation of pA-MM-$IspS_{ib}^{N397V\ A476V}$ and ptrc-low into *E. coli* BL21(DE3). Strains EISO07 and EISO08 were constructed using a similar strategy. The fermentation process and the quantification of isoprene were performed according to methods described in a previous report (4). After 0, 4, 8, 16, 20, 24, 28, 32, and 42 h of isopropyl-β-d-thiogalactopyranoside (IPTG) induction, 1 mL of the bacterial solution was obtained for SDS-PAGE analysis for protein expression detection (4).

RESULTS

Construction of tripartite protein folding sensor

In order to facilitate high-throughput analysis, a tripartite protein folding sensor that could monitor protein folding was constructed in the present study. The principle of the tripartite protein folding sensor is illustrated in Fig. 1. A guest protein, $IspS_{ib}$ (depicted in red in the figure), was inserted into the middle of a selectable marker named β-lactamase (depicted in cyan and blue), which conferred ampicillin resistance. $IspS_{ib}$ was

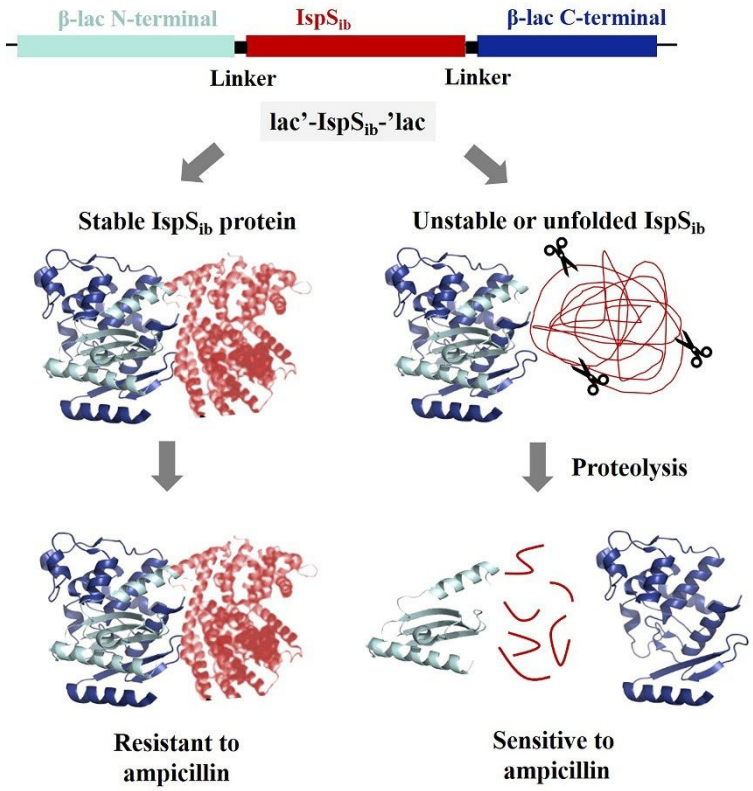

FIG 1 Schematic diagram of a tripartite system for the screening of improved $IspS_{ib}$ stability. $IspS_{ib}$ was inserted between residues 196 and 197 of β-lactamase, constructing a tripartite protein system, lac′-$IspS_{ib}$-′lac. If $IspS_{ib}$ is folded properly (left panel), namely, stable, it should bring the N- and C-terminal halves of β-lactamase close together, enabling β-lactamase to fold properly and thus giving ampicillin resistance. However, if $IspS_{ib}$ is poorly folded (right panel), it will be cleaved by proteases in the cell, and the N- and C-terminal halves of β-lactamase would be separated, resulting in sensitivity to ampicillin.

inserted into β-lactamase between residues 196 and 197, dividing β-lactamase into two fragments, N-terminal and C-terminal fragments, thereby generating a tripartite protein system that was designated as lac′-IspS$_{ib}$-′lac (Fig. 1). Residues 196 and 197 in β-lactamase were located at the surface-exposed loop, and the enzyme activity would not be affected if IspS$_{ib}$ was inserted at this site, similar to the insertion of Im7 into this site (18, 21). The concept was that if IspS$_{ib}$ was folded properly, it would bring the N-terminal and C-terminal fragments of β-lactamase close together, forming an intact fusion protein with high levels of ampicillin resistance (Fig. 1). However, if IspS$_{ib}$ was poorly folded, it would be cleaved by proteases in the cell, and the N-terminal and C-terminal fragments of β-lactamase would be separated, resulting in reduced resistance to ampicillin (Fig. 1). Therefore, the constructed tripartite protein folding system lac′-IspS$_{ib}$-′lac would couple the stability of IspS$_{ib}$ to antibiotic resistance.

Next, the plasmid pET-IspS$_{ib}$-lac containing the tripartite protein folding system lac′-IspS$_{ib}$-′lac was constructed (Fig. S1). The growth of *E. coli* BL21 (DE3) containing the pET-IspS$_{ib}$-lac plasmid was evaluated in a medium containing increasing concentrations of the antibiotic ampicillin (Fig. S2). In the first 2 h of culture, the same OD_{600} was obtained under different ampicillin concentrations, indicating that the expressed IspS$_{ib}$ was stable and conferred ampicillin resistance to the strain (Fig. S2B). After 2 h, the OD_{600} decreased in parallel to the concentration of ampicillin (Fig. S2B). This result indicated that the expressed IspS$_{ib}$ was degraded by the proteases in the cells after 2 h of culture, indicating the instability of the expressed IspS$_{ib}$, as described previously (4, 7). Without ampicillin (0 mg/L), the OD_{600} of the strain was not affected (Fig. S2B). Strain *E. coli* BL21 (DE3) containing an empty plasmid pET-28a, which was constructed for use as the negative control group, presented OD_{600} values that rarely increased in the medium containing ampicillin (Fig. S2A). Strain *E. coli* BL21 (DE3) containing the pET-IspS$_{ib}$-linker-lac or pET-lac-linker-IspS$_{ib}$ plasmid, constructed as the positive control, presented OD_{600} values that were not affected in the medium containing ampicillin (Fig. S2C and D). Therefore, it was inferred that the stability of IspS$_{ib}$ was successfully coupled with the antibiotic ampicillin resistance using the tripartite protein folding system lac′-IspS$_{ib}$-′lac.

The antibiotic resistance of the strain expressing the tripartite fusion lac′-IspS$_{ib}$-′lac was evaluated by spotting and spreading dilutions of cells onto plates containing media with different concentrations of ampicillin (Fig. S2E and F). When 40 mg/L of ampicillin was added to the medium, almost no clones were detected in the plates, indicating that the growth of the strain was inhibited at the 40 mg/L concentration of ampicillin.

Directed evolution of IspS$_{ib}$ to improve enzyme stability

Directed evolution is a strategy widely used for altering the characteristics of an enzyme. As stated above, the stability of IspS$_{ib}$ *in vivo* was successfully coupled to

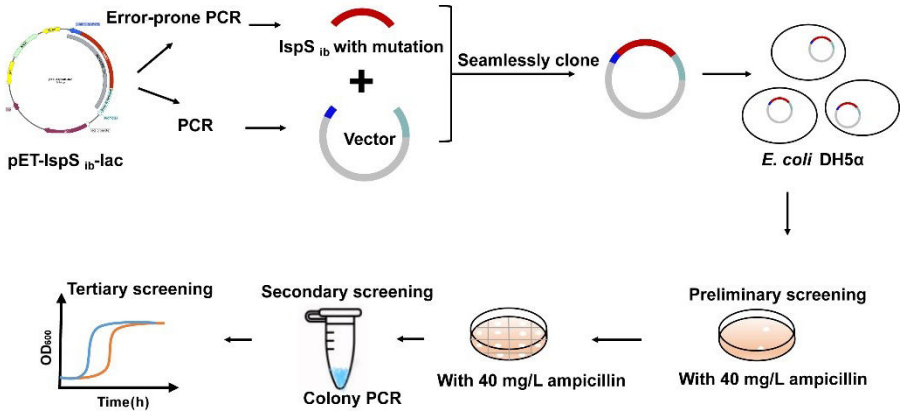

FIG 2 Directed evolution of IspS$_{ib}$ to improve thermostability. The mutant library was constructed by error-prone PCR. A three-step screening was performed to find the positive mutant.

ampicillin resistance, which provided a high-throughput screening method for selecting the high-stability variants. Therefore, to obtain variants of the $IspS_{ib}$ enzyme with high thermal stability, directed evolution was performed using the tripartite protein folding system lac′-$IspS_{ib}$-′lac as the method for high-throughput screening (Fig. 2). The $IspS_{ib}$ portion of the fusion construct lac′-$IspS_{ib}$-′lac was subjected to error-prone PCR, and the obtained mutated $IspS_{ib}$ fragments were assembled into the fusion construct, replacing the original wild-type $IspS_{ib}$. The resulting mutant library was transformed into *E. coli* DH5α, which was then plate-cultured on a medium containing 40 mg/L of ampicillin (Fig. S3A) for preliminary screening. The single clones were streaked using a sterile toothpick onto the medium containing 50 mg/L of kanamycin and 40 mg/L of ampicillin to confirm the cell growth (Fig. S3B). It was observed that the partial fragment of $IspS_{ib}$ in the fusion construct lac′-$IspS_{ib}$-′lac could be lost during the library construction process, resulting in a stable fusion construct exhibiting normal resistance to ampicillin and affecting the evaluation of positive clones. In order to prevent false positives, the obtained single clones were subjected to colony PCR to confirm the integrity of the fusion construct lac′-$IspS_{ib}$-′lac (secondary screening; Fig. S3C). The obtained positive clones were then subjected to cell growth monitoring in the fluid LB medium containing 50 mg/L of kanamycin and 40 mg/L of ampicillin, and the clones with high cell growth were selected (tertiary screening).

In the first round of directed evolution, the variant $IspS_{ib}^{V406A\ N397S\ T388A}$ with high cell growth was screened (Fig. 3A). In order to confirm the key mutation site among the three sites in this variant, each of these sites in the wild-type $IspS_{ib}$ was mutated separately, generating $IspS_{ib}^{V406A}$, $IspS_{ib}^{N397S}$, and $IspS_{ib}^{T388A}$. The cell growth results (Fig. 3B) indicated that the variant $IspS_{ib}^{N397S}$ exhibited the same enzyme stability as that of $IspS_{ib}^{V406A\ N397S\ T388A}$, confirming that N397S was the key mutation site among the three mutation sites. In order to further improve the enzyme's stability, N397 was mutated to the remaining 19 amino acids, thereby generating a saturation mutagenesis library. Variant $IspS_{ib}^{N397V}$

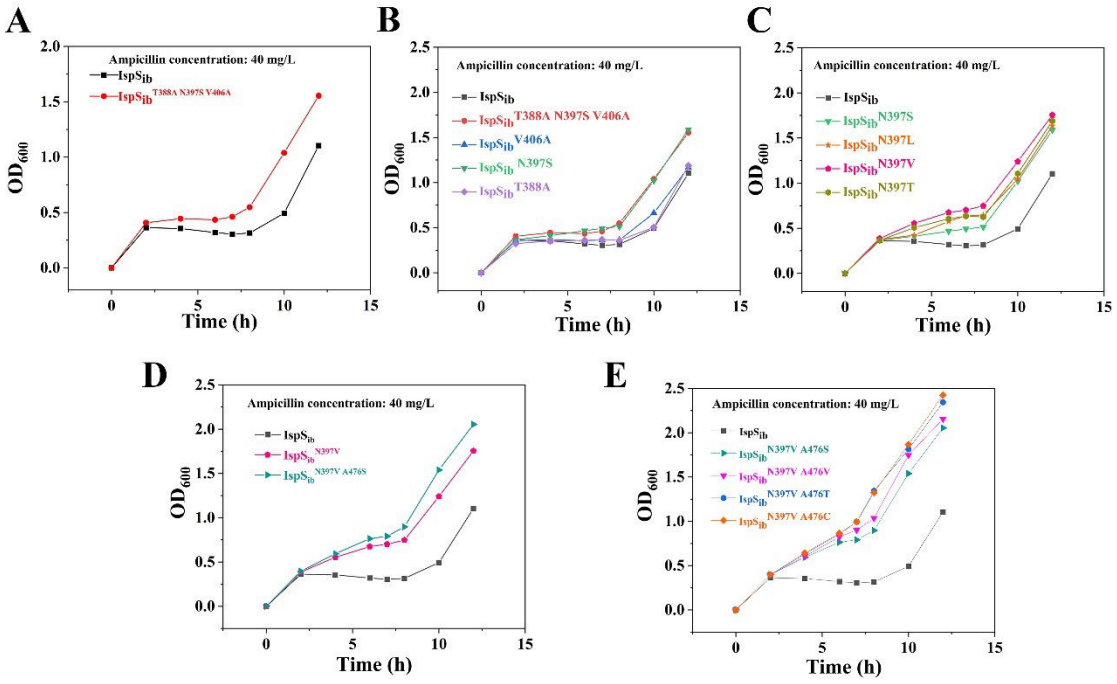

FIG 3 Cell growth of the wild-type $IspS_{ib}$ and $IspS_{ib}$ variants. The strains were cultivated in LB medium with 50 mg/L kanamycin and 40 mg/L ampicillin. Values are reported as the mean ± SD of triplicate experiments. (A) The cell growth of IspSib and variant IspSib T388A N397S V406A. (B) The cell growth of the wild-type IspSib and four variants of IspSibT388A N397S V406A, IspSibV406A, IspSibN397S and IspSibT388A. (C) The cell growth of the wild-type IspSib and four variants of IspSibN397S, IspSibN397L, IspSibN397V and IspSibN397T. (D) The cell growth of two variants of IspSibN397V, IspSibN397V A476S and the wild-type IspSib. (E) The cell growth of the wild-type IspSib and four variants of IspSibN397V A476S, IspSibN397V A476V, IspSibN397V A476T and IspSibN397V A476C.

exhibited the highest cell growth among all variants (Fig. 3C). The second round of directed evolution involved screening the variants $IspS_{ib}^{N397V}$ and $IspS_{ib}^{N397V\ A476S}$, which exhibited higher growth than the variant $IspS_{ib}^{N397V}$ at 40 mg/L of ampicillin (Fig. 3D). As described above, the A476 site in these variants was mutated to the remaining 19 amino acids, generating a saturation mutagenesis library. Three mutations, at A476V, A476T, and A476C, respectively, were revealed to result in improved cell growth (Fig. 3E). Finally, the corresponding three variants, $IspS_{ib}^{N397V\ A476V}$, $IspS_{ib}^{N397V\ A476T}$, and $IspS_{ib}^{N397V\ A476C}$, which were speculated to have improved enzyme stability, were obtained through the above two rounds of directed evolution and site saturation mutagenesis.

Thermostability test of wild-type $IspS_{ib}$ and the variants

The wild-type $IspS_{ib}$ and the screened variants ($IspS_{ib}^{N397V\ A476V}$, $IspS_{ib}^{N397V\ A476T}$, and $IspS_{ib}^{N397V\ A476C}$) were subjected to the estimation of thermostability *in vitro*. The enzymes were purified to the level of electrophoretic purity (Fig. S4). Subsequently, the purified enzymes were incubated at different temperatures (30°C, 40°C, and 50°C) for different durations, and the enzyme activity was determined to reflect the enzyme stability. The enzyme activity prior to heat exposure was defined as 100% activity (Fig. 4). After incubation at 30°C for 20 min, the variants $IspS_{ib}^{N397V\ A476V}$, $IspS_{ib}^{N397V\ A476T}$, and $IspS_{ib}^{N397V\ A476C}$ exhibited 65.60%, 36.45%, and 36.88% of the initial enzyme activity, respectively, all of which were higher than the wild-type $IspS_{ib}$ (21.03%) (Fig. 4). After incubation at 40°C for 20 min, no enzyme activity was detected for wild-type $IspS_{ib}$, while the variants $IspS_{ib}^{N397V\ A476V}$, $IspS_{ib}^{N397V\ A476T}$, and $IspS_{ib}^{N397V\ A476C}$ exhibited 40.47%, 36.71%, and 25.80% of the initial enzyme activity, respectively (Fig. 4). After incubation at 50°C for 10 min, no enzyme activity was detected for the wild-type $IspS_{ib}$ and the variant $IspS_{ib}^{N397V\ A476C}$,

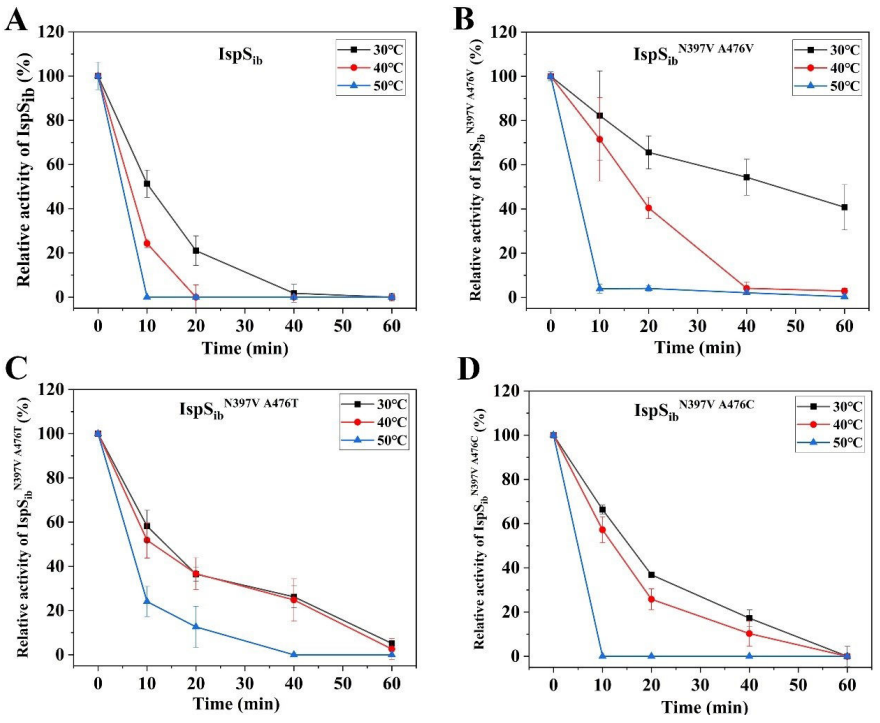

FIG 4 Thermostability test of the wild-type $IspS_{ib}$ and $IspS_{ib}$ variants. Thermostability was evaluated by measuring the enzyme activity after exposure at 30°C, 40°C, and 50 °C for 10, 20, 40, and 60 min. The enzyme activity before heat exposure was defined as 100%. Values are reported as the mean ± SD of triplicate experiments. (A) Thermostability test of the purified wild-type IspSib enzyme. (B) Thermostability test of the purified the variant IspSibN397V A476V enzyme. (C) Thermostability test of the purified the variant IspSibN397V A476T enzyme. (D) Thermostability test of the purified the variant IspSibN397V A476C enzyme.

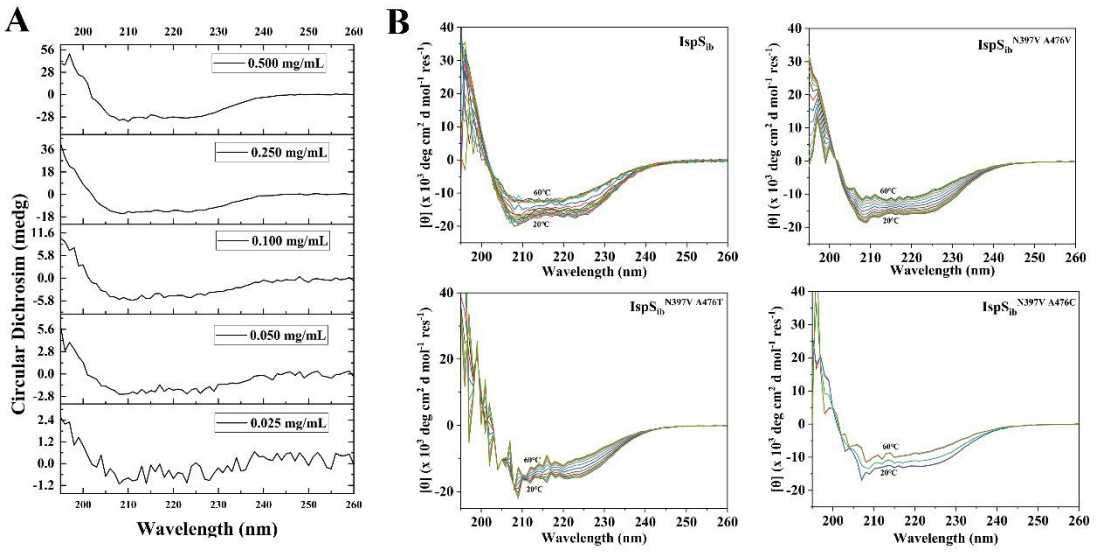

FIG 5 CD spectrum of the wild-type $IspS_{ib}$ and $IspS_{ib}$ variants. (A) Circular dichroism of the wild-type $IspS_{ib}$ at different concentrations, including 0.025, 0.050, 0.100, 0.250, and 0.500 mg/mL. (B) CD absorption spectra (mean residue ellipticity, [θ]) of wild-type $IspS_{ib}$ and $IspS_{ib}$ variants were recorded in the 195–260 nm range at a temperature range of 20°C-60°C, once per degree.

while 3.93% and 24.08% of the initial enzyme activity remained for the variants $IspS_{ib}^{N397V\ A476V}$ and $IspS_{ib}^{N397V\ A476T}$, respectively (Fig. 4). These data indicated that the screened variants exhibited higher thermal stability than the wild-type $IspS_{ib}$.

CD spectrum of wild-type $IspS_{ib}$ and the variants

The CD spectroscopic technique is widely used for estimating the secondary structures of proteins, that is, the percentage of residues in the secondary structures (α-helices, β-sheets, and random coils), and also the folding properties of proteins (22). The CD technique also reveals the kinetic and thermodynamic properties of the proteins, thereby enabling the evaluation of their conformation and stability and determining their melting temperatures (T_m) (23). Therefore, CD measurements conducted within a temperature range could be used to determine the effects of mutations on protein stability. In order to select the appropriate protein concentration for the CD analysis, five concentrations of wild-type $IspS_{ib}$, ranging from 0.025 to 0.500 mg/mL, were prepared and subjected to the estimation of T_m (Fig. 5A; Table 3). According to the results, a concentration of 0.25 mg/mL was selected for further analysis. The wild-type $IspS_{ib}$ and the variants were subjected to the determination of thermal stability using the CD spectra (195–260 nm) within the temperature range of 20°C–60°C, once per degree, with a 2°C/min rate of increase in the temperature. Fig. 5B depicts the CD spectra obtained at different temperatures. The T_m was estimated through the Global3 analysis of the CD spectra. The T_m values of the variants $IspS_{ib}^{N397V\ A476V}$, $IspS_{ib}^{N397V\ A476T}$, and $IspS_{ib}^{N397V\ A476C}$ were 45.1 ± 0.9°C, 46.1 ± 0.7°C, and 47.2 ± 0.3°C, respectively, and each of these values was higher than the T_m of wild-type $IspS_{ib}$ (41.5 ± 0.4°C) (Table 4). These data demonstrated that the variants had higher thermal stability than wild-type $IspS_{ib}$.

TABLE 3 T_m of wild-type $IspS_{ib}$ with different concentrations

Concentration of $IspS_{ib}$ (mg/mL)	0.025	0.050	0.100	0.250	0.500
T_m (°C)	30.6 ± 1.0	41.0 ± 0.5	41.1 ± 0.4	42.8 ± 0.2	44.8 ± 0.7

TABLE 4 T_m of wild-type $IspS_{ib}$ and the screened variants

Proteins	$IspS_{ib}$	$IspS_{ib}^{N397V\ A476V}$	$IspS_{ib}^{N397V\ A476T}$	$IspS_{ib}^{N397V\ A476C}$
T_m (°C)	41.5 ± 0.4	45.1 ± 0.9	46.1 ± 0.7	47.2 ± 0.3

Isoprene production in the engineered strains with $IspS_{ib}$ variants

Improvement of protein stability is rather challenging, as variants often interfere with protein function. Therefore, to further investigate the function of the $IspS_{ib}$ variants, the IspS variants were used for isoprene production in engineered *E. coli*. The original wild-type $IspS_{ib}$ in the pA-MM-$IspS_{ib}$ plasmid (4) was replaced with three $IspS_{ib}$ variants, generating pA-MM-$IspS_{ib}^{N397V\ A476V}$, pA-MM-$IspS_{ib}^{N397V\ A476T}$, and pA-MM-$IspS_{ib}^{N397V\ A476C}$, respectively (Table 2). Each of these four plasmids was then co-transformed with plasmid pYJM14 (6), which harbored *ERG12*, *ERG8*, *ERG19*, and IDI_{sc} from *Saccharomyces cerevisiae*, into *E. coli* BL21 (DE3), generating the strains EISO05, EISO06, EISO07, and EISO08, respectively (Table 2). Isoprene production was evaluated next (Fig. 6). The strains EISO06, EISO07, and EISO08 exhibited 1.42-, 1.94-, and 1.77-fold isoprene production compared to that of the control strain EISO05, with EISO07 exhibiting the highest isoprene production of 1,335 mg/L (Fig. 6). A summary of isoprene production in engineered strains reported in the last 10 years was prepared (Table 5). The *E. coli* strain AceCo with deletion of nine genes for achieving the reduced formation of byproducts from acetyl-CoA exhibited the highest isoprene production reported to date, 1,832 mg/L, which was nearly twofold higher than the control strain MGpsPtM constructed using *E. coli* MG1655 (2). The wild-type *E. coli* BL21 (DE3) was used for the construction of the strain EISO07 in the present study, and engineering of EISO07 to reduce the formation of byproducts similar to that for the published strain *E. coli* AceCo (2) might further increase isoprene production. Therefore, even though the isoprene production achieved in the present study was not the same or higher than the highest isoprene production reported to date, the strain EISO07 harboring the $IspS_{ib}^{N397V\ A476T}$ variant with higher thermal stability had the potential for further improvement.

In order to further confirm the stability of the screened variants *in vivo*, protein expression levels in the four strains were determined using SDS-PAGE at different time points after induction (Fig. 7). In strain EISO05, the levels of accumulated wild-type $IspS_{ib}$ protein were decreased at 16 h after induction, and almost no $IspS_{ib}$ protein was detected at 24 h after induction (Fig. 7). In strain EISO06, even though the levels of accumulated $IspS_{ib}^{N397V\ A476V}$ were decreased at 16 h after induction, the protein remained stable and could be observed even at 42 h after induction (Fig. 7). However, the appearance of a thin $IspS_{ib}^{N397V\ A476V}$ band at 16 h after induction indicated protein degradation, which might account for the relatively low-level increase in isoprene

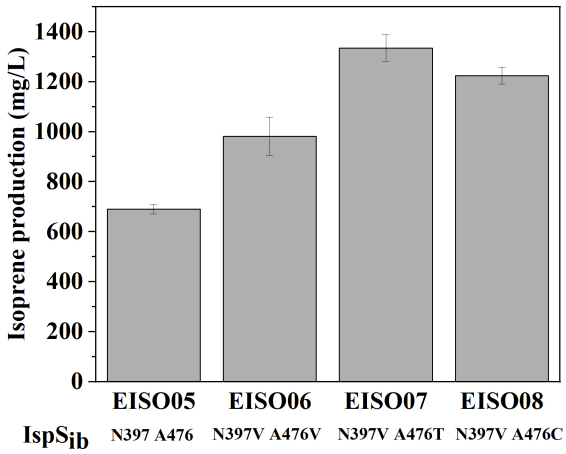

FIG 6 Isoprene production of the constructed strains. Values are reported as the mean ± SD of triplicate experiments.

TABLE 5 Summary of isoprene production in microbial cell factories

Host	Characteristics of main strategies	Content/production	Culture conditions	References
E. coli	Overexpression of IspS and MVA pathway	320 mg/L from glycerol	Shake-flask, 100 mL, 30 h	(24)
E. coli	EDP + PPP for precursor supply; overexpression of *ispS*, *idi*, *dxs*, and *ispG*	220.78 mg/L from glucose	Shake-flask, 40 mL, 48 h	(25)
E. coli	Overexpression of genes *dxs*, *dxr*, and *idi*	2.727 mg/g/h	Shake-flask, 2 mL, 2 h	(26)
E. coli	Antisense RNA strategy to weaken expression of ispA, ispB, and ispU	16 mg/L from glucose	Shake-flask, 3 mL, 20 h	(27)
E. coli	Reducing formation of byproducts from acetyl-CoA; overexpression of IspS and MVA pathway genes	1,832 mg/L from glycerol	Shake-flask, 50 mL, 36 h	(2)
E. coli	Directed co-evolution of DXS/DXR/IDI; promoter manipulation;	17.5 mg/L	Shake-flask, 5 mL, 2.5 h	(28)
E. coli	The synergy between the MEP pathway and the MVA pathway	629 mg/L from glucose; 24.0 g/L from glucose	Shake-flask, 10 mL, 24 h Fed-batch, 20 L, 48 h	(29)
E. coli	A novel MVA-mediated pathway	2.2 mg/L from glucose; 620 mg/L from glucose	Shake-flask, 50 mL, 24 h Fed-batch, 2.5 L, 32 h	(5)
E. coli	Overexpression of the MVA pathway and IspS; key enzymes screening; RBS optimization	698 mg/L from glucose	Shake-flask, 100 mL, 48 h	(4)
E. coli	Overexpression of the MVA pathway and IspS; controlling the expression levels of genes in MVA pathway; adding dodecane in cultures to release toxicity	587 ± 47 mg/L from glucose	Shake-flask, 1 mL, 44 h	(30)
E. coli	Test of different *E. coli* groups	25.2 ± 0.15 g/L from glycerol and yeast extract	Fed-batch, 300 L, 72 h	(11)
E. coli	Recycling redox cofactor by co-production of isoprene and 1,3-propanediol	665.2 mg/L from glucose	Shake-flask, 100 mL, 48 h	(31)
E. coli	Co-production of isoprene and lactate in microaerobic conditions	4.5 g/L from glucose and mevalonate	Fed-batch, 3 L, 45 h	(32)
E. coli	Modulation of the growth rate, acetate accumulation, and plasmid instability	18 g/L from glucose and yeast extract	Fed-batch, 1 L, 16 h	(33)
E. coli	D RNA scaffolds	609.3 ± 57.9 mg/L from glucose and acetate	Shake-flask, 4 mL, 48 h	(34)
E. coli	Overexpression of $IspS_{ib}$ with increased thermal stability; overexpression of the MVA pathway genes	1,335 mg/L from glucose	Shake-flask, 100 mL, 48 h	This study
Saccharomyces cerevisiae	Push-pull-restrain strategy for MVA pathway and acetyl-CoA pathways	37 mg/L from sucrose and glycerol	Shake-flask, 3 L, 72 h	(35)
S. cerevisiae	Cytoplasmic and mitochondrial acetyl-CoA utilization; overexpression of MVD1, IDI1, PMK, tHMG1, and ERG12, ERG10, and HMGS	246 mg/L from glucose 2,527 mg/L from sucrose	Shake-flask, 5 mL, 3 d Fed-batch, 2.5 L, 120 h	(36)
S. cerevisiae	Overexpression of *GAL4* to improve IspS expression; directed evolution of IspS to improve catalytic activity; increasing precursor supply	640 mg/L from sucrose; 3.7 g/L from glucose	Aerobic batch, 2.5 L, 72 h Fed-batch, 2.5 L, 96 h	(16)
Synechocystis	Overexpression of the MVA pathway and IspS	320 μg/L, 250 μg/g DCW from CO_2	Gaseous/aqueous two-phase photobioreactor, 700 mL, 196 h	(37)
Synechocystis	Overexpression of IDI and IspS	800 μg/L from CO_2	Gaseous-aqueous two-phase reactor, 700 mL, 95 h	(38)
Synechococcus elongatus	Fusion of IDI and IspS	1.26 g/L from CO_2	Photobioreactor, 20 mL, 21 d	(39)
Synechocystis	*cpcB*IspS* fusion	5.4 mg/g DCW; 2.5 mg/L from CO_2	Gaseous-aqueous two-phase bioreactor, 700 mL, 96 h	(40)

(*Continued on next page*)

TABLE 5 Summary of isoprene production in microbial cell factories (*Continued*)

Host	Characteristics of main strategies	Content/production	Culture conditions	References
In vitro production	Balanced enzyme unit (0.5 μM of MVK, PMK, MVD; 1.0 μM of IDI, 8.0 μM of ISPS	302 mg/L from mevalonate	50 mL, 40 h	(41)
Bacillus subtilis DSM 402	Overexpression of Kudzu isoprene synthase	1434.3 μg/L	Shake-flask, 2 mL, 48 h	(42)
Bacillus licheniformis DSM 13	Overexpression of Kudzu isoprene synthase	437.2 μg/L	Shake-flask, 2 mL, 48 h	(42)
Clostridium ljungdahlii	Overexpression of Idi and IspS	10 μg/L from fructose; 1.98 μg/L from syngas	1 d in 10 mL of MES-F medium at 37°C; 20 h in 10 mL of MES-0F medium at 30°C	(43)
Chlamydomonas reinhardtii	Overexpression of *Ib*IspS, *Cr*BKT and *Sc*IDI	362 mg/L from acetic acid	6 d cultivation in 1 mL medium at 30°C in light conditions of 12 h:12 h light:dark cycle	(44)

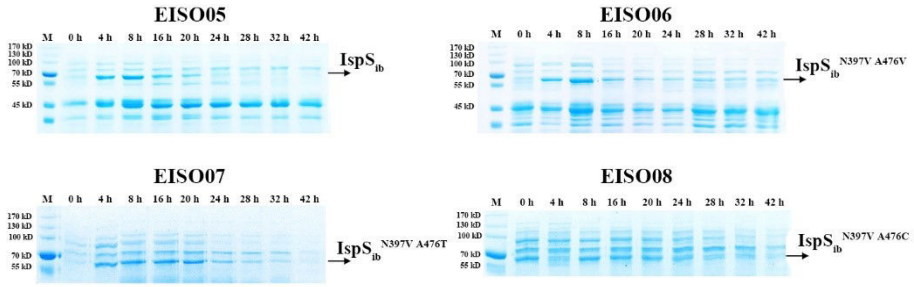

FIG 7 SDS-PAGE analysis of protein expression after induction in isoprene-producing strains. M: molecular weight marker; 0–40 h: number of hours after induction.

production (just 1.42-folds) in strain EISO06 among the three strains. In strains EISO07 and EISO08, the bands for IspS$_{ib}^{N397V\ A476T}$ and IspS$_{ib}^{N397V\ A476C}$ proteins were detected even at 42 h after induction, indicating increased stability in these strains. In strain EISO07, the band for protein IspS$_{ib}^{N397V\ A476T}$ was evidently darker than the other protein bands until 20 h after induction. However, in strain EISO08, almost no decrease in the levels of IspS$_{ib}^{N397V\ A476C}$ was observed during the fermentation process, and the band for IspS$_{ib}^{N397V\ A476C}$ was not the darkest. Therefore, it was inferred that, at the early stage of the fermentation process, higher IspS$_{ib}$ protein accumulation occurred in strain EISO07 than in strain EISO08, which led to slightly higher isoprene production in EISO07. In conclusion, these SDS-PAGE data demonstrated the improved stability of each of the three IspS$_{ib}$ variants *in vivo*.

DISCUSSION

Variation in the enzyme characteristics of IspS is rarely reported. Rational design of IspS is also rarely reported due to a lack of information on the crystal structure and the catalytic reaction mechanism of this enzyme. Studies on the directed evolution of IspS are also limited owing to the difficulty of performing the high-throughput screening method. Isoprene is a colorless compound that is released in gaseous form during microbial fermentation and renders it difficult to perform the product-based high-throughput screening method. Two putative substrate-based high-throughput screening methods to improve enzyme activity are reported. The substrate named DMAPP is reportedly cytotoxic (8, 45). According to a study, the enzyme activity of IspS was positively correlated with DMAPP cytotoxicity relief, which manifested as improved cell growth (16). Using this screening method, a positive variant of ISPSM4, which resulted in a twofold increase in isoprene production, was obtained (16). In another study, a novel DMAPP-responding genetic circuit sensor based on an L-arabinose operon was developed (46). The L-arabinose ligand-binding domain of AraC in the operon was replaced with an IspS gene, enabling the binding of DMAPP to the AraC-IspS complex. The catalytic activity of IspS could be positively correlated to the expression level of GFP through this sensor (46). However, this sensor has not been applied successfully to date for the directed evolution of IspS to obtain positive variants. No other study, to the best of the authors' knowledge, has been reported so far on the screening and evolution of IspS.

The present study pioneered the construction of a tripartite protein folding system that coupled the stability of IspS$_{ib}$ to antibiotic resistance, followed by the successful application of this system for the directed evolution of IspS$_{ib}$ to improve the stability of this enzyme. In the screening step, the 40 mg/L concentration of ampicillin was selected for plate screening, unlike previous studies, which simplified the screening process. In a previously published study, a range of ampicillin concentrations were tested (18). Another highlight of the present study was the use of colony PCR to confirm the integrity of the fusion construct of the screened clones and eliminate false-positive clones. The colony PCR results indicated that most of the clones obtained after preliminary screening

were false-positive clones (Fig. S3C). Therefore, the colony PCR step used in the present study would shorten the entire screening process. In summary, the directed evolution process used in the present study to improve enzyme stability was efficient.

Terpene synthases catalyze the key cyclization step in the formation of various terpenoids (or isoprenoids), which represent the single largest class of natural compounds that are valued highly as drugs, fragrances, food additives, colorants, biofuels, and in rubber manufacturing (8). Terpene synthases typically exhibit low activity and thermostability, and protein engineering is required to improve the properties of these enzymes prior to using them in industrial applications (47). However, protein engineering of terpene synthases is difficult as it requires an appropriate high-throughput assay for screening mutant libraries. In a study, a farnesyl diphosphate analog named synthetic substrate 3 was designed for screening the cyclization reactions catalyzed by the sesquiterpene synthase BcBOT2, which increased the thermostability by 12°C (48). Other enzyme properties, such as enzyme activity, substrate affinity, cofactor preference, and product inhibition, could also be optimized using these high-throughput screening methods based on synthetic substrate 3 (48). However, this synthetic substrate 3 could only be used for optimizing the properties of sesquiterpene synthase, while its application to most terpene synthases was limited. On the other hand, the tripartite protein folding system constructed in the present study is applicable for optimizing the thermostability of most terpene synthases.

According to reports, the C-terminal of terpene synthases might be related to their thermostability. In a previous study, the naturally thermostable terpene synthases (RoseRS_3509 and Rcas_0622) derived from thermophilic organisms were revealed to have a significantly truncated C-terminus relative to SSCG_03688, a mesophile muurolol synthase (49). This truncation of the C-terminals of terpene synthases relative to SSCG_03688 resulted in increased thermostability without negatively affecting the enzyme activity (49). In another study, the directed evolution of terpene synthase caused the most thermostable variant 19B7 to lose its three C-terminal amino acids (48). Interestingly, in the present study, the mutation sites of the screened variant were N397 and A476, both located within the C-terminal of $IspS_{ib}$. The present study, therefore, indicated that sites N397 and A476 of $IspS_{ib}$ play a key role in the thermostability of this enzyme. According to the alignment results, in all the IspS enzymes from different species, the N and A residues were located within the homologous sites 397 and 476, respectively (10), indicating the conservation of these two sites.

In summary, a tripartite protein folding system, lac′-$IspS_{ib}$-′lac, which could couple the stability of $IspS_{ib}$ to antibiotic resistance, was successfully constructed in the present study. The directed evolution of $IspS_{ib}$ was then performed through two rounds of random mutation and site-saturation mutation, which generated three variants with higher stability: $IspS_{ib}^{N397V\ A476V}$, $IspS_{ib}^{N397V\ A476T}$, and $IspS_{ib}^{N397V\ A476C}$. The thermostability test and the CD analysis confirmed the increased protein stability. Isoprene production was also increased when using these variants. The strain EISO07 exhibited the highest isoprene production of 1,335 mg/L. The findings of the present study would serve as a successful example of improving enzyme stability without requiring detailed structural information or the catalytic reaction mechanism. The tripartite protein folding system and the high-throughput process developed in the present study could be used as templates for other enzymes. The present study provides fresh insights into the optimization of the thermostability of terpene synthases, which are key enzymes for the production of isoprenoids in engineered microorganisms.

ACKNOWLEDGMENTS

This work was supported by grants from the Natural Science Foundation of Shandong Province, China (ZR2022QB143, ZR2020QC069), the National Natural Science Foundation of China (22278233), the State Key Laboratory of Microbial Technology Open Projects Fund (M2022-07, M2023-05), the "First class grassland science discipline" program in Shandong Province, the Talents of High Level Scientific Research Foundation (grants

6651120032, 6651117005, and 6651121004) of Qingdao Agricultural University, and the CAS Key Laboratory of Biobased Materials, Qingdao Institute of Bioenergy and Bioprocess Technology, Chinese Academy of Sciences (BMF-2020-01).

The authors would also like to thank the "Laboratory for Agricultural Molecular Biology" for providing laboratory apparatus.

The authors declare that they have no known competing financial interests or personal relationships that could have appeared to influence the work reported in this paper.

No conflict of interest exists in the submission of this manuscript, and manuscript is approved by all authors for publication.

AUTHOR AFFILIATIONS

[1]Energy-rich Compound Production by Photosynthetic Carbon Fixation Research Center, Shandong Key Lab of Applied Mycology, College of Life Sciences, Qingdao Agricultural University, Qingdao, Shandong, China
[2]Key Laboratory of Biobased Materials, Qingdao Institute of Bioenergy and Bioprocess Technology, Chinese Academy of Sciences, Qingdao, Shandong, China
[3]Shandong Energy Institute, Qingdao, Shandong, China
[4]Qingdao New Energy Shandong Laboratory, Qingdao, Shandong, China
[5]State Key Laboratory of Microbial Technology, Shandong University, Qingdao, Shandong, China

AUTHOR ORCIDs

Meijie Li http://orcid.org/0000-0003-0129-8059
Jianming Yang http://orcid.org/0000-0002-3268-211X

FUNDING

Funder	Grant(s)	Author(s)
山东省科学技术厅 | Natural Science Foundation of Shandong Province (山东省自然科学基金)	ZR2022QB143	Meijie Li
MOST | National Natural Science Foundation of China (NSFC)	22007091	Meijie Li

ADDITIONAL FILES

The following material is available online.

Supplemental Material

Supplemental materials (AEM01218-23-S0001.docx). Supplemental materials and methods, Fig. S1 to S4.

REFERENCES

1. Claeys M, Graham B, Vas G, Wang W, Vermeylen R, Pashynska V, Cafmeyer J, Guyon P, Andreae MO, Artaxo P, Maenhaut W. 2004. Formation of secondary organic aerosols through photooxidation of isoprene. Science 303:1173–1176. https://doi.org/10.1126/science.1092805
2. Kim JH, Wang C, Jang HJ, Cha MS, Park JE, Jo SY, Choi ES, Kim SW. 2016. Isoprene production by *Escherichia coli* through the exogenous mevalonate pathway with reduced formation of fermentation byproducts. Microb Cell Fact 15:214. https://doi.org/10.1186/s12934-016-0612-6
3. Whited GM, Feher FJ, Benko DA, Cervin MA, Chotani GK, McAuliffe JC, LaDuca RJ, Ben-Shoshan EA, Sanford KJ. 2010. Technology update: development of a gas-phase bioprocess for isoprene-monomer production using metabolic pathway engineering. Ind Biotechnol 6:152–163. https://doi.org/10.1089/ind.2010.6.152
4. Li M, Chen H, Liu C, Guo J, Xu X, Zhang H, Nian R, Xian M. 2019. Improvement of isoprene production in *Escherichia coli* by rational optimization of RBSs and key enzymes screening. Microb Cell Fact 18:4. https://doi.org/10.1186/s12934-018-1051-3
5. Yang J, Nie Q, Liu H, Xian M, Liu H. 2016. A novel MVA-mediated pathway for isoprene production in engineered *E. coli*. BMC Biotechnol 16:5. https://doi.org/10.1186/s12896-016-0236-2
6. Yang J, Xian M, Su S, Zhao G, Nie Q, Jiang X, Zheng Y, Liu W, Williams SJ. 2012. Enhancing production of bio-isoprene using hybrid MVA pathway and isoprene synthase in *E.coli*. PLoS One 7:e33509. https://doi.org/10.1371/journal.pone.0033509
7. Li M, Liu C, Chen H, Deng L, Zhang H, Nian R, Xian M. 2019. Biochemical characterization of isoprene synthase from *Ipomoea batatas*. J Biosci Bioeng 127:138–144. https://doi.org/10.1016/j.jbiosc.2018.07.022

8. Li M, Hou F, Wu T, Jiang X, Li F, Liu H, Xian M, Zhang H. 2020. Recent advances of metabolic engineering strategies in natural isoprenoid production using cell factories. Nat Prod Rep 37:80–99. https://doi.org/10.1039/c9np00016j
9. Yang J, Zhao G, Sun Y, Zheng Y, Jiang X, Liu W, Xian M. 2012. Bio-isoprene production using exogenous MVA pathway and isoprene synthase in *Escherichia coli*. Bioresour Technol 104:642–647. https://doi.org/10.1016/j.biortech.2011.10.042
10. Li M, Nian R, Xian M, Zhang H. 2018. Metabolic engineering for the production of isoprene and isopentenol by *Escherichia coli*. Appl Microbiol Biotechnol 102:7725–7738. https://doi.org/10.1007/s00253-018-9200-5
11. Lee H-W, Park J-H, Kim W-K, Lee J-G, Lee J-S, Ahn J-O, Lee E-G, Lee H-W. 2020. Engineered *Escherichia coli* strains as platforms for biological production of isoprene. FEBS Open Bio 10:780–788. https://doi.org/10.1002/2211-5463.12829
12. Schnitzler J-P, Zimmer I, Bachl A, Arend M, Fromm J, Fischbach RJ. 2005. Biochemical properties of isoprene synthase in poplar (populus x canescens). Planta 222:777–786. https://doi.org/10.1007/s00425-005-0022-1
13. Sinha R, Shukla P. 2019. Current trends in protein engineering: updates and progress. Curr Protein Pept Sci 20:398–407. https://doi.org/10.2174/1389203720666181119120120
14. Song Z, Zhang Q, Wu W, Pu Z, Yu H. 2023. Rational design of enzyme activity and enantioselectivity. Front Bioeng Biotechnol 11:1129149. https://doi.org/10.3389/fbioe.2023.1129149
15. Köksal M, Zimmer I, Schnitzler J-P, Christianson DW. 2010. Structure of isoprene synthase illuminates the chemical mechanism of teragram atmospheric carbon emission. J Mol Biol 402:363–373. https://doi.org/10.1016/j.jmb.2010.07.009
16. Wang F, Lv X, Xie W, Zhou P, Zhu Y, Yao Z, Yang C, Yang X, Ye L, Yu H. 2017. Combining Gal4P-mediated expression enhancement and directed evolution of isoprene synthase to improve isoprene production in *Saccharomyces cerevisiae*. Metab Eng 39:257–266. https://doi.org/10.1016/j.ymben.2016.12.011
17. Sachsenhauser V, Bardwell JC. 2018. Directed evolution to improve protein folding *in vivo*. Curr Opin Struct Biol 48:117–123. https://doi.org/10.1016/j.sbi.2017.12.003
18. Foit L, Morgan GJ, Kern MJ, Steimer LR, von Hacht AA, Titchmarsh J, Warriner SL, Radford SE, Bardwell JCA. 2009. Optimizing protein stability *in vivo*. Mol Cell 36:861–871. https://doi.org/10.1016/j.molcel.2009.11.022
19. Guan A, Mei K, Lv M, Lu J, Lou Q, Yang W. 2018. The effect of electron beam irradiation on IgG binding capacity and conformation of tropomyosin in shrimp. Food Chem 264:250–254. https://doi.org/10.1016/j.foodchem.2018.05.051
20. Kelly SM, Jess TJ, Price NC. 2005. How to study proteins by circular dichroism. Biochim Biophys Acta 1751:119–139. https://doi.org/10.1016/j.bbapap.2005.06.005
21. Galarneau A, Primeau M, Trudeau L-E, Michnick SW. 2002. β-lactamase protein fragment complementation assays as *in vivo* and *in vitro* sensors of protein–protein interactions. Nat Biotechnol 20:619–622. https://doi.org/10.1038/nbt0602-619
22. Greenfield NJ. 2006. Using circular dichroism spectra to estimate protein secondary structure. Nat Protoc 1:2876–2890. https://doi.org/10.1038/nprot.2006.202
23. Corrêa D, Ramos C. 2009. The use of circular dichroism spectroscopy to study protein folding, form and function. Afr J Biochem Res 3:164–173.
24. Zurbriggen A, Kirst H, Melis A. 2012. Isoprene production via the mevalonic acid pathway in *Escherichia coli* (bacteria). Bioenerg. Res 5:814–828. https://doi.org/10.1007/s12155-012-9192-4
25. Liu H, Sun Y, Ramos KRM, Nisola GM, Valdehuesa KNG, Lee W, Park SJ, Chung W-J, Parish T. 2013. Combination of entner-doudoroff pathway with MEP increases isoprene production in engineered *Escherichia coli*. PLoS One 8:e83290. https://doi.org/10.1371/journal.pone.0083290
26. Lv X, Xu H, Yu H. 2013. Significantly enhanced production of Isoprene by ordered coexpression of genes *dxs*, *dxr*, and *idi* in *Escherichia coli*. Appl Microbiol Biotechnol 97:2357–2365. https://doi.org/10.1007/s00253-012-4485-2
27. Liu C-L, Lv Q, Tan T-W. 2015. Joint antisense RNA strategies for regulating isoprene production in *Escherichia coli*. RSC Adv 5:74892–74898. https://doi.org/10.1039/C5RA12161B
28. Lv X, Gu J, Wang F, Xie W, Liu M, Ye L, Yu H. 2016. Combinatorial pathway optimization in *Escherichia coli* by directed co-evolution of rate-limiting enzymes and modular pathway engineering. Biotechnol Bioeng 113:2661–2669. https://doi.org/10.1002/bit.26034
29. Yang C, Gao X, Jiang Y, Sun B, Gao F, Yang S. 2016. Synergy between methylerythritol phosphate pathway and mevalonate pathway for isoprene production in *Escherichia coli*. Metab Eng 37:79–91. https://doi.org/10.1016/j.ymben.2016.05.003
30. Liu CL, Bi HR, Bai Z, Fan LH, Tan TW. 2019. Engineering and manipulation of a mevalonate pathway in *Escherichia coli* for isoprene production. Appl Microbiol Biotechnol 103:239–250. https://doi.org/10.1007/s00253-018-9472-9
31. Guo J, Cao Y, Liu H, Zhang R, Xian M, Liu H. 2019. Improving the production of isoprene and 1,3-propanediol by metabolically engineered *Escherichia coli* through recycling redox cofactor between the dual pathways. Appl Microbiol Biotechnol 103:2597–2608. https://doi.org/10.1007/s00253-018-09578-x
32. Cheng T, Liang X, Wang Y, Chen N, Feng D, Liang F, Xie C, Liu T, Zou H. 2021. Co-production of isoprene and lactate by engineered *Escherichia coli* in microaerobic conditions. Molecules 26:23. https://doi.org/10.3390/molecules26237173
33. Joshi H, Isar J, Jain DA, Badle SS, Dhoot SB, Rangaswamy V. 2021. C/N ratio and specific growth rate plays important role on enhancing isoprene production in recombinant *Escherichia coli*. Appl Biochem Biotechnol 193:2403–2419. https://doi.org/10.1007/s12010-021-03545-5
34. Liu C-L, Dong H-G, Xue K, Sun L, Yang Y, Liu X, Li Y, Bai Z, Tan T-W. 2022. Metabolic engineering mevalonate pathway mediated by RNA scaffolds for mevalonate and isoprene production in *Escherichia coli*. ACS Synth Biol 11:3305–3317. https://doi.org/10.1021/acssynbio.2c00226
35. Lv X, Xie W, Lu W, Guo F, Gu J, Yu H, Ye L. 2014. Enhanced isoprene biosynthesis in *Saccharomyces cerevisiae* by engineering of the native acetyl-CoA and mevalonic acid pathways with a push-pull-restrain strategy. J Biotechnol 186:128–136. https://doi.org/10.1016/j.jbiotec.2014.06.024
36. Lv X, Wang F, Zhou P, Ye L, Xie W, Xu H, Yu H. 2016. Dual regulation of cytoplasmic and mitochondrial acetyl-CoA utilization for improved isoprene production in *Saccharomyces cerevisiae*. Nat Commun 7:12851. https://doi.org/10.1038/ncomms12851
37. Bentley FK, Zurbriggen A, Melis A. 2014. Heterologous expression of the mevalonic acid pathway in cyanobacteria enhances endogenous carbon partitioning to isoprene. Mol Plant 7:71–86. https://doi.org/10.1093/mp/sst134
38. Chaves JE, Romero PR, Kirst H, Melis A. 2016. Role of isopentenyl-diphosphate isomerase in heterologous cyanobacterial (*Synechocystis*) isoprene production. Photosynth Res 130:517–527. https://doi.org/10.1007/s11120-016-0293-3
39. Gao X, Gao F, Liu D, Zhang H, Nie X, Yang C. 2016. Engineering the methylerythritol phosphate pathway in cyanobacteria for photosynthetic isoprene production from CO_2. Energy Environ. Sci 9:1400–1411. https://doi.org/10.1039/C5EE03102H
40. Chaves JE, Rueda-Romero P, Kirst H, Melis A. 2017. Engineering isoprene synthase expression and activity in cyanobacteria. ACS Synth Biol 6:2281–2292. https://doi.org/10.1021/acssynbio.7b00214
41. Cheng T, Liu H, Zou H, Chen N, Shi M, Xie C, Zhao G, Xian M. 2017. Enzymatic process optimization for the *in vitro* production of isoprene from mevalonate. Microb Cell Fact 16:8. https://doi.org/10.1186/s12934-016-0622-4
42. Gomaa L, Loscar ME, Zein HS, Abdel-Ghaffar N, Abdelhadi AA, Abdelaal AS, Abdallah NA. 2017. Boosting isoprene production via heterologous expression of the kudzu isoprene synthase gene (*klspS*) into *Bacillus* spp. cell factory. AMB Express 7:161. https://doi.org/10.1186/s13568-017-0461-7
43. Diner BA, Fan J, Scotcher MC, Wells DH, Whited GM. 2018. Synthesis of heterologous mevalonic acid pathway enzymes in *Clostridium ljungdahlii* for the conversion of fructose and of syngas to mevalonate and isoprene. Appl Environ Microbiol 84:e01723-17. https://doi.org/10.1128/AEM.01723-17

44. Yahya RZ, Wellman GB, Overmans S, Lauersen KJ. 2023. Engineered production of isoprene from the model green microalga *Chlamydomonas reinhardtii* Metab Eng Commun 16:e00221. https://doi.org/10.1016/j.mec.2023.e00221
45. George KW, Thompson MG, Kim J, Baidoo EEK, Wang G, Benites VT, Petzold CJ, Chan LJG, Yilmaz S, Turhanen P, Adams PD, Keasling JD, Lee TS. 2018. Integrated analysis of isopentenyl pyrophosphate (IPP) toxicity in isoprenoid-producing *Escherichia coli*. Metab Eng 47:60–72. https://doi.org/10.1016/j.ymben.2018.03.004
46. Liu CL, Cai JY, Bi HR, Tan TW. 2018. A novel DMAPP-responding genetic circuit sensor for high-throughput screening and evolving isoprene synthase. Appl Microbiol Biotechnol 102:1381–1391. https://doi.org/10.1007/s00253-017-8676-8
47. Siddiqui KS. 2015. Some like it hot, some like it cold: temperature dependent biotechnological applications and improvements in extremophilic enzymes. Biotechnol Adv 33:1912–1922. https://doi.org/10.1016/j.biotechadv.2015.11.001
48. Lauchli R, Rabe KS, Kalbarczyk KZ, Tata A, Heel T, Kitto RZ, Arnold FH. 2013. High-throughput screening for terpene-synthase-cyclization activity and directed evolution of a terpene synthase. Angew Chem Int Ed Engl 52:5571–5574. https://doi.org/10.1002/anie.201301362
49. Styles MQ, Nesbitt EA, Marr S, Hutchby M, Leak DJ. 2017. Characterization of the first naturally thermostable terpene synthases and development of strategies to improve thermostability in this family of enzymes. FEBS J 284:1700–1711. https://doi.org/10.1111/febs.14072